Journal of Solid State Chemistry 183 (2010) 871–877

Contents lists available at ScienceDirect

Journal of Solid State Chemistry

journal homepage: www.elsevier.com/locate/jssc

Hybrid materials of SBA-16 functionalized by rare earth (Eu^{3+}, Tb^{3+}) complexes of modified β-diketone (TTA and DBM): Covalently bonding assembly and photophysical properties

Yajuan Li, Bing Yan *, Ying Li

Department of Chemistry, Tongji University, Siping Road 1239, Shanghai 200092, China

ARTICLE INFO

Article history:
Received 8 November 2009
Received in revised form
31 January 2010
Accepted 7 February 2010
Available online 16 February 2010

Keywords:
Organic–inorganic hybrids
Rare earth ion
Luminescence
Covalently bonded mesoporous host

ABSTRACT

Novel mesoporous SBA-16 type of hybrids TTA-S16 and DBM-S16 were synthesized by co-condensation of modified β-diketone (TTA-Si and DBM-Si, DBM=1,3-diphenyl-1,3- propanepione, TTA=2-thenoyltrifluoroacetone) and tetraethoxysilane (TEOS) in the presence of Pluronic F127 as template, which were confirmed by FTIR, XRD, ^{29}Si CP-MAS NMR, and N_2 adsorption measurements. Novel organic–inorganic mesoporous luminescent hybrid containing RE^{3+} (Eu^{3+}, Tb^{3+}) complexes covalently attached to the functionalized ordered mesoporous SBA-16 (TTA-S16 and DBM-S16), which were designated as bpy-*RE*-TTA-S16 and bpy-*RE*-DBM-S16, were obtained by sol–gel process. The luminescence properties of these resulting materials were characterized in detail, and the results reveal that mesoporous hybrid material bpy-Eu-TTA-S16 present stronger luminescent intensities, longer lifetimes, and higher luminescent quantum efficiencies than the corresponding DBM-containing materials bpy-Eu-DBM-S16, while bpy-Tb-DBM-S16 exhibit the stronger characteristic emission of Tb^{3+} and longer lifetime than the corresponding TTA-containing materials bpy-Tb-TTA-S16.

© 2010 Elsevier Inc. All rights reserved.

1. Introduction

Organic–inorganic hybrid materials have been attracting a great deal of attention because of their extraordinary properties as they not only combine the beneficial properties of the inorganic and organic components in a single material, but also often exhibit exceptional properties that exceed what would be expected for a simple mixture of the components [1,2]. To date, sol–gel process, which is based on hydrolysis and polycondensation reactions, is one of the most commonly employed methods for the preparation of inorganic–organic hybrid materials. The major advantages of the process are its simplicity, mild reaction conditions, and ability to control the purity and homogeneity of the final materials at the nanomolecular scale [3]. Moreover, the microstructure, the external shape, or the degree of combination of the organic and the inorganic phases can be further controlled by modifying the sol–gel process conditions [4–6]. It is well known that rare-earth ions have sharp and intense emission bands based on their *f–f* electronic transitions and a wide range of luminescent lifetimes, suitable for various applications, but they have low absorption coefficients, limiting the lighting output. However, this can be improved by forming complexes of the rare-earth ions with organic ligands that strongly absorb light and transfer the energy to the metal center (antenna effect) [7–10]. Interest in rare-earth-containing organic–inorganic hybrids has grown considerably during the last decade, which is mainly due to the fact that they combine the intrinsic characteristics of sol–gel derived hosts and the luminescence features of trivalent rare-earth ions [8]. Much previous work has been done on physical mixing methods. However, these hybrid materials have many disadvantages such as the doping concentration of a complex silica matrix is very low and it is hard to obtain transparent and uniform material. Poor mechanical properties also restrict its practical application [11,12]. As a consequence, another appealing method of synthesizing hybrid materials containing covalent bonds has emerged, and the as-derived molecular-based materials show improved chemical stability and have a monophasic appearance similar in nature to that of the complicated molecular polymeric Si–O network [13,14]. In recent years, our research group have dedicated to covalently grafting the ligands to the inorganic networks in which rare earth complexes luminescent centers are bonded with a siloxane matrix through Si–O linkage using different modified routes, including modification of active amino group, hydroxyl groups, and carboxyl groups with coupling agent, etc. [6,15–18]. These studies indicate that the thermal stabilities and photophysical properties of the rare-earth complexes were improved by the matrices. So far, incorporation of luminescent rare earth complexes in solid matrices is of

* Corresponding author. Fax: +86 21 65982287.
E-mail address: byan@tongji.edu.cn (B. Yan).

0022-4596/$ - see front matter © 2010 Elsevier Inc. All rights reserved.
doi:10.1016/j.jssc.2010.02.006

widespread interest in materials science as it allows construction of functional materials with various optical properties.

In addition, the luminescence properties of *RE* organic complexes supported on surfactant-templated mesostructures have been the subject of many research works, since their photophysical properties may be modified by interaction with the mesoporous host structure [19]. In recent years, many research groups have paid attention to the modification of the mesoporous materials with rare earth complexes, and the synthesis and luminescence properties of a serial of SBA-15/MCM-41 mesoporous materials covalently bonded with rare earth complexes have been reported [19–24]. However, recently much fascinating interest has been altered to the synthesis of ordered silica SBA-16 materials with cage-like mesopores in the mesoporous material field [25], which can also be functionalized by rare earth complexes through covalent bonding [26].

In this manuscript, we extended our previous approach and synthesized two kinds of β-diketone functionalized SBA-16 mesoporous hybrid materials (TTA-S16 and DBM-S16), in which 2-thenoyltrifluoroacetone (TTA) and 1,3-diphenyl-1,3-propanepione (DBM) were covalently bonded to the framework of SBA-16 by co-condensation of the modified organic groups (denoted as TTA-Si and DBM-Si) and the tetraethoxysilane (TEOS) by using Pluronic F127 as template. The highly luminescent ternary rare earth (Eu^{3+}, Tb^{3+}) complexes on functionalized SBA-16 with modified β-diketone ligands (denoted as bpy-*RE*-TTA-S16 and bpy-*RE*-DBM-S16, *RE*=Eu, Tb) were obtained by introducing RE^{3+} and 2,2′-bipyridine (bpy) into the TTA-S16 and DBM-S16 hybrid materials through covalent bond assembling method. Full characterization and detail studies of luminescence properties of all these synthesized materials were investigated in relation to guest–host interactions between the organic complex and the silica matrix.

2. Experimental section

2.1. Chemicals

Europium and terbium nitrates were obtained by dissolving their respective oxides (Eu_2O_3 and Tb_4O_7) in concentrated nitric acid. 3-(Triethoxysilyl)-propyl isocyanate (TEPIC) was purchased from Lancaster Synthesis Ltd. Tetraethoxysilane (TEOS) was distilled and stored under a N_2 atmosphere. The solvent tetrahydrofuran (THF) was used after desiccation with anhydrous calcium chloride. Other starting reagents were used as received.

2.2. Synthesis

2.2.1. Synthesis of TTA-functionalized SBA-16 mesoporous material (TTA-S16)

The modified precursor TTA-Si was synthesized according to the procedure reported in the literature [19], described as follows: firstly, 1 mmol 2-thenoyltrifluoroacetone (TTA) was dissolved in 20 mL of dehydrate tetrahydrofuran (THF), and NaH (2 mmol, 0.048 g) was added into the solution with stirring. Two hours later, 2.0 mmol (0.495 g) of 3-(triethoxysilyl)-propyl-isocyanate (TEPIC) was then put into the solution by drops for half an hour. The whole mixture was refluxing at 60 °C under argon for approximately 12 h. A yellow oil sample i.e. the precursor TTA-Si was furnished after isolation and purification. The mesoporous material TTA-S16 was synthesized from acidic mixture with the following molar composition: 0.0040 F127: 0.96 TEOS: 0.04 TTA-Si: 4 HCl: 130 H_2O. F127 (0.508 g) was firstly dissolved in the deionized water (3.4 g) and 2 M HCl solution (20 g) at 35 °C under vigorous stirring. A mixture of TEOS and TTA-Si was added into the above solution, which was further stirred at 35 °C for 24 h and transferred into a Teflon bottle sealed in an autoclave, which was then heated at 100 °C for 24 h. The solid product was recovered by filtration, washed thoroughly with deionized water, and air-dried at room temperature. Removal of copolymer surfactant F127 was conducted by Soxhlet extraction with ethanol for 48 h. The material was dried in a vacuum and showed a light-yellow color.

2.2.2. Synthesis of DBM-functionalized SBA-16 mesoporous material (DBM-S16)

The synthesis procedure of DBM-S16 was similar to that of TTA-S16 except that TTA was replaced by DBM.

2.2.3. Synthesis of SBA-16 mesoporous material covalently bonded with the ternary RE^{3+} complexes (denoted as bpy-RE-TTA-S16 and bpy-RE-DBM-S16, respectively. RE=Eu, Tb)

The sol–gel-derived hybrid mesoporous material bpy-*RE*-TTA-S16 was prepared as follows: while being stirred, TTA-S16 was soaked in an appropriate amount of $RE(NO_3)_3$ and 2,2′-bipyridine (bpy) ethanol solution with the molar ratio of RE^{3+}:TTA-S16:bpy=1:3:1. The mixture was stirred at room temperature for 12 h followed by filtration and extensive washing with EtOH. The resulting material bpy-*RE*-TTA-S16 was dried at 60 °C under vacuum overnight. The predicted structure of bpy-*RE*-TTA-S16 was obtained as outlined in Fig. S1.

The synthesis procedure for bpy-*RE*-DBM-S16 was similar to that of bpy-*RE*-TTA-S16 except TTA-S16 was replaced by DBM-S16. And the predicted structure of bpy-*RE*-DBM-S16 was obtained as outlined in Fig. S2.

2.3. Characterization

FTIR spectra were measured within the 4000–400 cm^{-1} region on an infrared spectrophotometer with the KBr pellet technique. X-ray powder diffraction patterns were recorded on a Rigaku D/max-rB diffractometer equipped with a Cu anode in a 2θ range from 0.6° to 6°. Nitrogen adsorption/desorption isotherms were measured at the liquid nitrogen temperature, using a Nova 1000 analyzer. Surface areas were calculated by the Brunauer–Emmett–Teller (BET) method and pore size distributions were evaluated from the desorption branches of the nitrogen isotherms using the Barrett–Joyner–Halenda (BJH) model. ^{29}Si MAS NMR spectra were recorded at 79.46 MHz, using a Bruker Avance 400 spectrometer. Scanning electronic microscope (SEM) was measured on Philips XL30 operated. Transmission electron microscope (TEM) experiments were conducted on a JEOL2011 microscope operated at 200 kV or on a JEM-4000EX microscope operated at 400 kV. The fluorescence excitation and emission spectra were obtained on a Perkin-Elmer LS-55 spectrophotometer. Luminescence lifetime measurements were carried out on an Edinburgh FLS920 phosphorimeter using a 450 w xenon lamp as excitation source. Thermogravimetric analysis (TGA) was performed on a Netzsch STA 409 at a heating rate of 15 °C/min under nitrogen atmosphere.

3. Results and discussion

3.1. β-Diketones-functionalized parent materials (TTA-S16 and DBM-S16)

The presence and preservation of organic groups in TTA-S16 or DBM-S16 materials could be proved by the characterization of FTIR. Fig. 1 depicts the FTIR spectra of TTA-Si (a), DBM-Si (b),

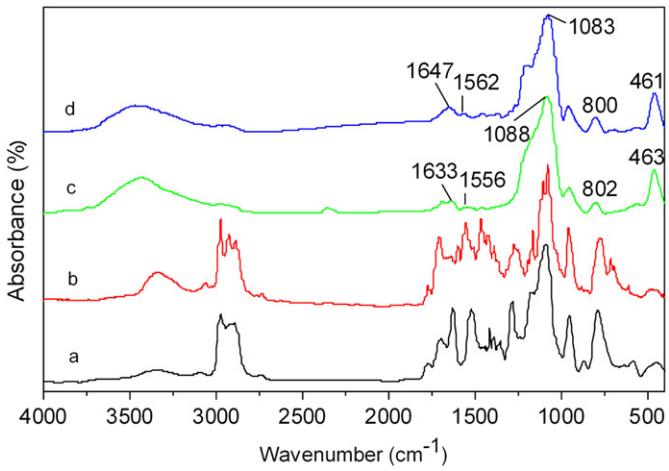

Fig. 1. FTIR spectra of TTA-Si (a), DBM-Si (b), β-diketone-functionalized mesoporous materials TTA-S16 (c) and DBM-S16 (d).

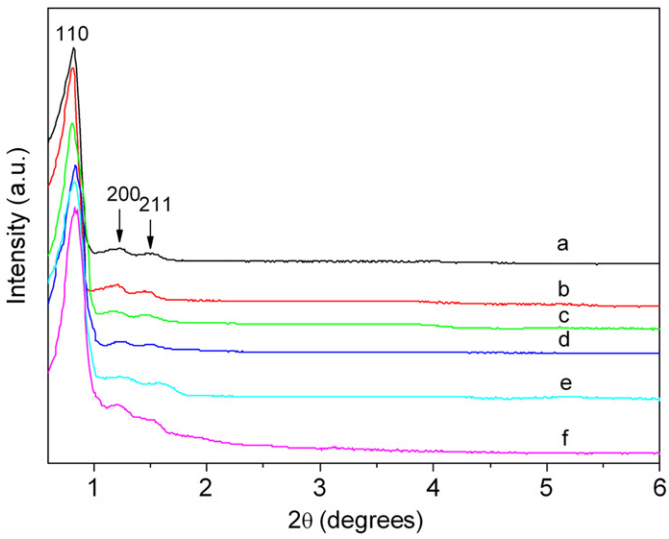

Fig. 2. SAXRD patterns of TTA-S16 (a), DBM-S16 (b), bpy-Eu-TTA-S16 (c), bpy-Tb-TTA-S16 (d), bpy-Eu-DBM-S16 (e) and bpy-Eu-DBM-S16 (f).

β-diketone-functionalized mesoporous materials TTA-S16 (c) and DBM-S16 (d). The formation of Si–O–Si is evidenced by the characteristic bands located at 1088, 1083 cm^{-1} with the shoulder at 1192 cm^{-1} (ν_{as}, Si–O–Si), 802, 800 cm^{-1} (ν_s, Si–O–Si), and 463, 461 cm^{-1} (δ, Si–O–Si) (ν represents stretching, δ in-plane bending, *s* symmetric, and *as* asymmetric vibrations). A peak at about 1455 cm^{-1} is attributed to out-of-plane rocking ω (Si–C). Bands at 1633 and 1556 cm^{-1}, originating from the –CONH– group of modified organic ligands, can also be observed in hybrid mesoporous materials TTA-S16 and DBM-S16, which indicates that TTA-Si and DBM-Si were successfully incorporated into both materials and preserved well after both hydrolysis-condensation reaction and the surfactant extraction procedure [22].

Fig. 2(a) and (b) exhibit the small-angle X-ray patterns of β-diketone-functionalized mesoporous materials TTA-S16 and DBM-S16, respectively. It can be seen that both samples exhibit three well-resolved diffraction peaks in the 2θ range of 0.6–2°, which are indexed as the (110), (200), and (211) diffractions, characteristic of SBA-16-type three-dimensional cubic (*Im3m*). This observation indicates that the highly ordered mesostructures of SBA-16-type were obtained. At the same time, the corresponding unit cell

Table 1
Structural parameters of TTA-S16, DBM-S16, bpy-*RE*-TTA-S16 and bpy-*RE*-DBM-S16 (*RE*=Eu, Tb)[a].

Sample	d_{110} (nm)	a_0 (nm)	D (nm)	t (nm)	S_{BET} (m^2/g)	V (cm^3/g)
TTA-S16	10.21	14.44	3.89	8.62	511	0.43
bpy-Eu-TTA-S16	10.34	14.62	2.63	10.03	446	0.31
bpy-Tb-TTA-S16	10.38	14.68	2.67	10.04	481	0.32
DBM-S16	10.34	14.62	3.55	9.11	519	0.46
bpy-Eu-DBM-S16	10.64	15.04	2.82	10.20	358	0.22
bpy-Tb-DBM-S16	10.64	15.04	2.54	10.48	366	0.23

[a] d_{100} is the d(110) spacing, a_0 the cell parameter ($a_0=\sqrt{2}\,d_{110}$), S_{BET} the BET surface area, V the total pore volume, D_{BJH} the average pore diameter, and t the wall thickness, calculated by $\sqrt{3}a_0/2-D_{BJH}$.

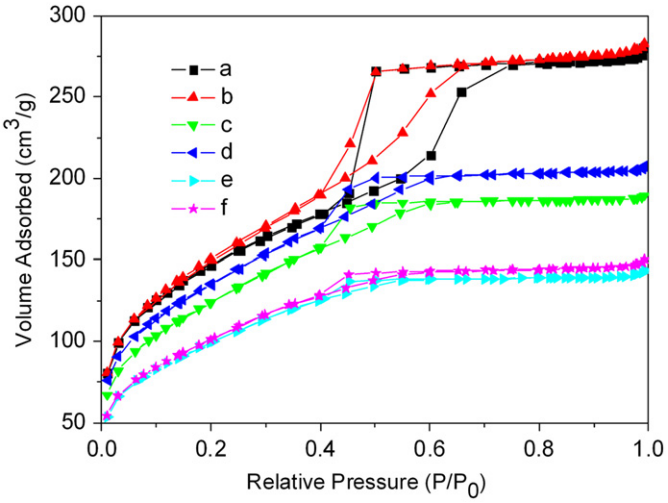

Fig. 3. N_2 adsorption–desorption isotherms for TTA-S16 (a), DBM-S16 (b), bpy-Eu-TTA-S16 (c), bpy-Tb-TTA-S16 (d), bpy-Eu-DBM-S16 (e) and bpy-Eu-DBM-S16 (f).

parameters a ($a=d_{hkl}/(h^2+k^2+l^2)^{1/2}$) of TTA-S16 and DBM-S16 materials were calculated and are listed in Table 1.

In order to further investigate the cage structure of TTA-S16 and DBM-S16 materials, the characterization of the nitrogen adsorption–desorption was also carried out. The corresponding isotherms are presented in Fig. 3 (a for TTA-S16 and b for DBM-S16). Both materials exhibit the type IV isotherms with H2-type hysteresis loops according to the IUPAC classification, typical for materials with ink-bottle pores with interconnectivity in a 3D pore system as a result of cavitation [27]. The specific area and pore size have been calculated using Brunauer–Emmett–Teller (BET) and Barrett–Joyner–Halenda (BJH) methods, respectively. The structure data of all these mesoporous materials (BET surface area, total pore volume, and pore size, etc.) are summarized in Table 1. From d, S_{BET}, and V of TTA-S16 and DBM-S16, it is worth noting that the data for both materials are less than those typically reported for pure SBA-16 mesoporous silica material [28]. This is probably due to the presence of organic ligand TTA (DBM) on the pore surface and the co-surfactant effect of TTA-Si (DBM-Si), which interacts with surfactant and reduces the diameter of the micelles.

3.2. Rare earth (RE^{3+}) complexes covalently bonded to TTA (DBM)-functionalized mesoporous SBA-16

In the resulting organic–inorganic mesoporous luminescent hybrid bpy-*RE*-TTA-S16 and bpy-*RE*-DBM-S16, The modified

ligands were covalently bonded to the SBA-16 host like an arm through Si–O–Si by the hydrolysis-condensation of organic functionality (TTA-Si and DBM-Si). There are two possible reasons for the proposed structure and coordination number. The one reason is that the rare earth positive ions are Lewis hard acid, so it is easy to coordinate with the hard base containing the oxygen and nitrogen atoms. And most of the rare earth complexes hold the polar covalent bonds, since the rare earth ions always make bonding through the 6*s*, 6*p* and 5*d* electronic orbits, whose total amount is nine. Therefore, it is the most stable for the rare earth complex to exist with the coordination number of eight or nine. And the other reason is that in the experiment we synthesize the material by adding the appropriate and accurate proportion of reagents into the system and we make the fixed stoichiometric ratio [Eu^{3+}:TTA-S16 (DBM-S16):bpy=1:3:1] in order to obtain the fixed model of rare earth complex. Furthermore, in view of the spatial stearic hindrance effect, we predicted the optimum coordination structure for RE^{3+} complex (Figs. S1 and S2).

Fig. 2(c–f) shows the powder XRD pattern of all obtained ternary mesoporous hybrids ((c) bpy-Eu-TTA-S16; (d) bpy-Tb-TTA-S16; (e) bpy-Eu-DBM-S16; (f) bpy-Tb-DBM-S16). It can be observed that all ternary hybrid materials still preserve well the typical XRD pattern of SBA-16-type, including a strong (110) reflections at a low angle and two small diffractions (200) and (211) at higher angles, indicating that the ordered cubic mesoporous structure of SBA-16 remains intact after introduction of RE^{3+}. However, it is worth noting that these ternary lanthanide mesoporous hybrids bpy-*RE*-TTA-S16 and bpy-*RE*-DBM-S16 appear decreasing in diffraction intensity as compared with the parent TTA-S16 and DBM-S16 materials, respectively. This is probably due to X-ray absorption/scatter by the RE^{3+} ions.

The characterization of N_2 adsorption–desorption for bpy-*RE*-TTA-S16 and bpy-*RE*-DBM-S16 materials further provides proof of the preservation of the mesoporous structure after the introduction of the RE^{3+} ion. As shown in Fig. 3, the typical type-IV isotherms with H2-type hysteresis loops of mesoporous materials for both samples still remain, similar to those of the corresponding parent materials. The structure parameters of both materials (d, S_{BET}, V, etc.) are summarized in Table 1. It can be observed that the values of the S_{BET}, D and v of materials after introducing RE^{3+} are less than those of TTA-S16 (DBM-S16), which further confirmed incorporation of the RE^{3+} complexes in the channels of SBA-16.

Figs. 4 and 5 presents the SEM and TEM images of pure SBA-16 (a) and the resulting mesoporous hybrid bpy-Eu-TTA-S16 (b), respectively. It can be seen that the morphology of pure SBA-16 is spherical and particle size is about 1 μm in diameter, while the mesoporous hybrid bpy-Eu-TTA-S16 shows an irregular cubic morphology with the size of about 1.5–2 μm, which may be due to the coexistence of organic and inorganic groups on the surface. The TEM images of SBA-16 and mesoporous hybrid bpy-Eu-TTA-S16 show well-ordered uniform mesoscopic array in three dimensional pores. But compared to pure SBA-16, the slight

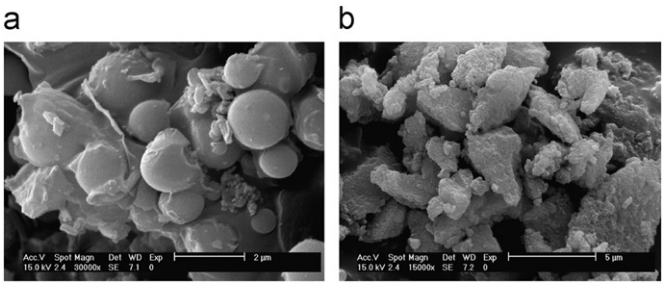

Fig. 4. SEM images of pure SBA-16 (a) and mesoporous hybrid bpy-Eu-TTA-S16 (b).

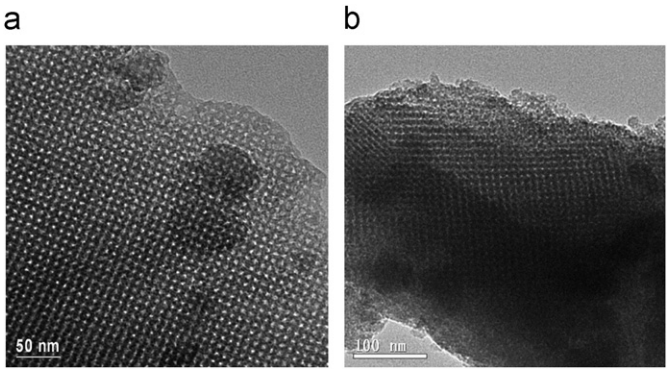

Fig. 5. TEM images of pure SBA-16 (a) and mesoporous hybrid bpy-Eu-TTA-S16 (b).

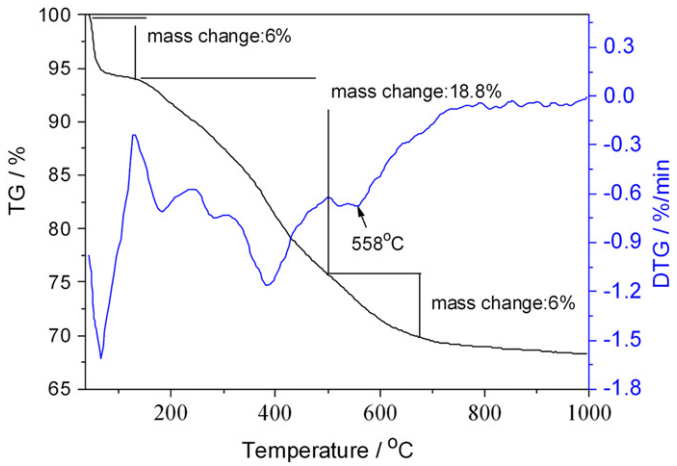

Fig. 6. TGA (-) and DTG (---) curves of bpy-Eu-DBM-S16.

decrease in ordering degree of mesoporous hybrid bpy-Eu-TTA-S16 is ascribed to the lanthanide complex anchored on the mesoporous surface. In addition, the distance between the centers of the mesopores for bpy-Eu-TTA-S16 is estimated to be about 10 nm, which is in good agreement with the values determined from the corresponding XRD analysis (see Table 1).

To investigate the thermal stability of all obtained ternary mesoporous hybrids, the thermogravimetric analysis (TGA) were carried out at a heating rate of 15 °C/min under nitrogen atmosphere. TG analysis shows that the thermal decomposition behavior of all these ternary mesoporous hybrids was similar, so we present the thermogravimetric weight loss curve (TGA) and derivative weight loss (DTG) curve of mesoporous hybrid bpy-Eu-DBM-S16 as an example (see Fig. 6). Three main weight loss peaks can be observed from the TG curve. A weight loss of ca. 6.0% below 125 °C is due to the physically adsorbed water and residue ethanol. A followed weight loss (approximately 18.8%) between 125 and 502 °C can be attributed to the decomposition of incompletely removed surfactant. The third weight loss (approximately 6.0%) between 502 and 675 °C is mostly ascribed to the decomposition of organic europium complex, corresponding to a main peak centered at 558 °C in DTG curve. At higher temperature, the weight loss can be ascribed to the condensation of some terminal Si–OH groups on the silica surface to form Si–O–Si networks. In addition, compared with the weight loss peak (approximately 68% at about 350 °C) of pure complex $Eu(DBM)_3bpy$ (see Supporting information Fig. S5), the decomposition point of bpy-Eu-DBM-S16 was higher than that of pure $Eu(DBM)_3bpy$, indicating that the thermal stability of the

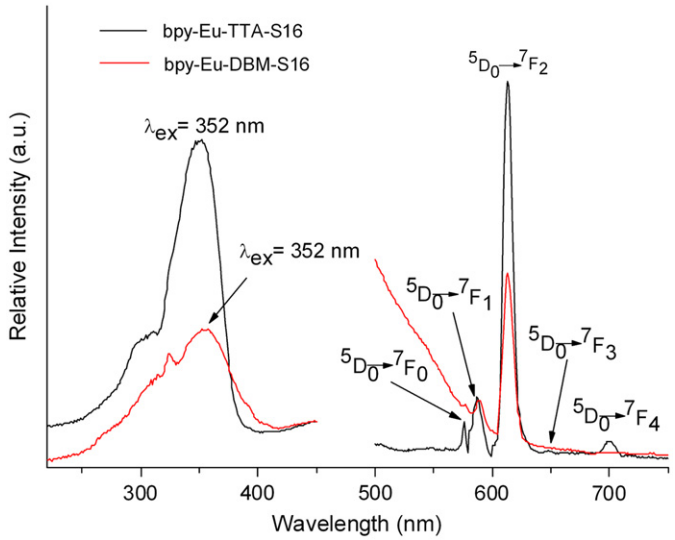

Fig. 7. Fluorescent excitation and emission spectra of the mesoporous hybrid material bpy-Eu-TTA-S16 and bpy-Eu-DBM-S16.

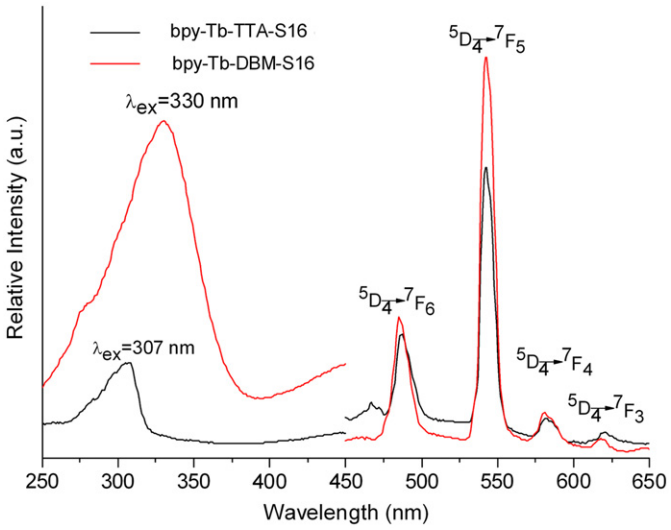

Fig. 8. Fluorescent excitation and emission spectra of the mesoporous hybrid materials bpy-Tb-TTA-S16 and bpy-Tb-DBM-S16.

rare earth complex was enhanced as it was covalently bonded to the mesoporous matrix.

3.3. Luminescence properties

The fluorescent excitation and emission spectra of mesoporous materials bpy-Eu-TTA-S16 and bpy-Eu-DBM-S16 are given in Fig. 7. The excitation spectra were obtained by monitoring the emission of Eu^{3+} ions at 613 nm and dominated by a series of broad bands centered at about 352 nm in the ultraviolet region, which are attributed to the $\pi \rightarrow \pi^*$ electron transition of the ligands. As a result, for hybrid bpy-Eu-TTA-S16, five main emission peaks centered at 576, 587, 613, 648, and 702 nm, corresponding to $^5D_0 \rightarrow {}^7F_J$ transitions (J=0, 1, 2, 3, 4) were obtained, while in mesoporous hybrid bpy-Eu-DBM-S16, only $^5D_0 \rightarrow {}^7F_J$ (J =0, 1, 2) transitions at 577, 589 and 613 nm were obtained, the $^5D_0 \rightarrow {}^7F_3$ and $^5D_0 \rightarrow {}^7F_4$ transitions are so weak that they cannot be clearly seen from the emission spectra of the sample, which is not a surprise because the poor energy level match has been described in this paper previously. A prominent feature that may be noted in these spectra is the high intensity ratio of $I(^5D_0 \rightarrow {}^7F_2)/I(^5D_0 \rightarrow {}^7F_1)$. The intensity (the integration of the luminescent band) ratio of the $^5D_0 \rightarrow {}^7F_2$ transition to the $^5D_0 \rightarrow {}^7F_1$ transition has been widely used as an indicator of Eu^{3+} site symmetry [29,30]. When interactions of the rare earth complex with its local chemical environment are stronger, the complex becomes more nonsymmetrical and the intensity of the electric-dipolar transitions becomes more intense. As a result, the $^5D_0 \rightarrow {}^7F_1$ transition (magnetic-dipolar transition) decreased and the $^5D_0 \rightarrow {}^7F_2$ transition (electric-dipolar transition) increased. The intensity ratio of the two lines ($^5D_0 \rightarrow {}^7F_2/{}^5D_0 \rightarrow {}^7F_1$) in the two hybrid bpy-Eu-TTA-S16 and the bpy-Eu-DBM-S16 is about 5.44 and 2.88, respectively, which indicates that the lanthanide ion is not at the center of an asymmetric coordination field. It is clear that strong coordination interactions took place between the organic groups and rare-earth ions.

Fig. 8 shows the excitation and emission spectra of bpy-Tb-TTA-S16 and bpy-Tb-DBM-S16 hybrid material, both of which are monitored at 545 nm at room temperature. The spectra exhibit broad excitation centered at 307 and 330 nm, respectively, corresponding to the ligand-to-metal charge-transfer (CT) transition caused by interaction between the organic groups and the rare-earth ions [31,32]. No apparent f–f transitions could be observed in the spectra. The wide CT excitation bands will benefit the energy transfer and luminescence to terbium ions. Besides, the excitation spectrum of bpy-Tb-DBM-S16 shows a broader band range and a stronger intensity than that of bpy-Tb-TTA-S16, which suggests that DBM is a better energy match with Tb^{3+} than TTA. From their emission spectra, characteristic Tb^{3+} ion emissions are observed. Bands in the 450–650 nm range can be clearly seen, which are assigned to the $^5D_4 \rightarrow {}^7F_J$ (J=3, 4, 5, 6) transitions at 487, 543, 581 and 620 nm. The mesoporous hybrid materials show relatively strong emissions due to the chemically covalently bonded molecular Si–O network structure between the complexes and the mesoporous silica. Besides, the luminescent intensity of bpy-Tb-DBM-S16 is slightly higher than that of bpy-Tb-TTA-S16, suggesting that the energy match between DBM and Tb^{3+} is more suitable than that between TTA and Tb^{3+}. In addition, we compared the $^5D_0$ quantum efficiency (η) of bpy-Eu-TTA-S16 with that of ternary mesoporous hybrid $Eu(TTA)_3$phen-SBA-15 [33], and it is found that the η value of former (19.0%) is much lower than that of the latter (37.6%), which may be attributed to the fact that nonradiative (k_{nr}) transition probability is higher in hybrid bpy-Eu-TTA-S16.

The typical decay curves of the Eu^{3+} and Tb^{3+} mesoporous hybrid materials were measured, and they can be described as a single exponential ($\mathrm{Ln}[S(t)/S_0] = -k_1 t = -t/\tau$), indicating that all Eu^{3+} and Tb^{3+} ions occupy the same average coordination environment. The resulting lifetime data of the Eu^{3+} and Tb^{3+} hybrids are given in Table 2. It was found that the luminescent lifetime of bpy-Eu-TTA-S16 (474.4 μs) is longer than that of bpy-Eu-DBM-S16 (306.4 μs), while it is contrary to the luminescent lifetimes of bpy-Tb-TTA-S16 (346.4 μs) and bpy-Tb-DBM-S16 (705.0 μs), which can be ascribed to the prediction from the energy match between TTA and DBM and Eu^{3+} (Tb^{3+}) ions. Because the main energy donor in the hybrid systems originates from the photoactive TTA and DBM functional groups, the energy match between the TTA and DBM functional groups is the most important factor determining the luminescent lifetimes of the corresponding hybrid materials. The energy match between DBM and Tb^{3+} is more suitable than that between TTA and Tb^{3+} because the energy difference $\Delta E(\mathrm{Tr} - \mathrm{Tb}^{3+})$ of DBM (3500 cm^{-1}) is better than that of TTA (100 cm^{-1}) according to the above

Table 2
Luminescence data of the mesoporous hybrid materials.

System	v_{01} (cm^{-1})	v_{02} (cm^{-1})	I_{02}/I_{01}	τ (μs)[a,b]	$1/\tau(s^{-1})$	A_r (s^{-1})	A_{nr} (s^{-1})	η (%)
bpy-Eu-TTA-S16	17036	16313	5.44	474.4[a]	2108	400.7	1707.3	19.0
bpy-Eu-DBM-S16	16978	16313	2.88	306.4[a]	3264	250.1	3013.9	7.66
bpy-Tb-TTA-S16				346.4[b]				
bpy-Tb-DBM-S16				705.0[b]				

[a] For the $^5D_0 \rightarrow {}^7F_2$ transition of Eu^{3+}.
[b] For the $^5D_4 \rightarrow {}^7F_5$ transition of Tb^{3+}.

discussion. The energy difference of TTA ($100\,cm^{-1}$) is too small to worsen the energy match, which easily produces the inverse energy loss to decrease the luminescent behavior. Similarly, the energy difference $\Delta E(Tr-Eu^{3+})$ of DBM ($4980\,cm^{-1}$) is worse than that of TTA ($1380\,cm^{-1}$) and is so large that it decreases the energy transfer from the triplet state of DBM to Eu^{3+}, so the energy match between DBM and Eu^{3+} is less suitable than that between TTA and Eu^{3+}. So, the luminescent lifetime data for these rare-earth covalently bonded hybrids correspond to the above prediction.

On the basis of the emission spectra and lifetimes of the $^5D_0$ emitting level, we selectively determined the emission quantum efficiencies of the $^5D_0$ excited state of europium ion for Eu^{3+} hybrids. Assuming that only nonradiative and radiative processes are essentially involved in the depopulation of the $^5D_0$ excited state, η can be defined as follows [34]:

$$\eta = A_r/(A_r + A_{nr}) \quad (1)$$

Here A_r and A_{nr} are radiative and nonradiative transition rates, respectively. A_r can also be obtained by summing over the radiative rates A_{0J} for each $^5D_0 \rightarrow {}^7F_J$ ($J=0-4$) transitions. The branching ratio for the $^5D_0 \rightarrow {}^7F_{5,6}$ transitions can be neglected as they are not detected experimentally, whose influence can be ignored in the depopulation of the $^5D_0$ excited state. Since $^5D_0 \rightarrow {}^7F_1$ belongs to the isolated magnetic dipole transition, it is practically independent of the chemical environments around Eu^{3+}, and can be considered as an internal reference for the whole spectra, the experimental coefficients of spontaneous emission A_{0J} can be calculated according to the equation [35–38] as follows:

$$A_{0J} = A_{01}(I_{0J}/I_{01})(v_{01}/v_{0J}) \quad (2)$$

Here A_{0J} is the experimental coefficients of spontaneous emission. A_{01} is Einstein's coefficient of spontaneous emission between the $^5D_0$ and $^7F_1$ energy levels. In vacuum A_{01} could be used as a value of $14.65\,s^{-1}$, while in the air atmosphere the value of A_{01} can be determined to be $50\,s^{-1}$ approximately ($A_{01}=n^3A_{01(vac)}$) [39], when an average index of refraction n equal to 1.506 was considered. I_{01} and I_{0J} are the integrated intensities of the $^5D_0 \rightarrow {}^7F_1$ and $^5D_0 \rightarrow {}^7F_J$ transitions (J=0–4) with v_{01} and v_{0J} ($v_{0J}=1/\lambda_J$) energy centers, respectively. v_{0J} refers to the energy barrier and can be determined with the emission peaks of Eu^{3+}'s $^5D_0 \rightarrow {}^7F_J$ emission transitions. The emission intensity, I, taken as integrated intensity of the $^5D_0 \rightarrow {}^7F_{0-4}$ emission curves.

On the basis of the above discussion, the quantum efficiencies of the two kinds of europium mesoporous hybrid materials can be determined in the order: bpy-Eu-TTA-S16 > bpy-Eu-DBM-S16, which takes agreement with the order of lifetimes. From the equation of η, it can be seen the value η mainly depends on two quantum values: one is lifetime and the other is I_{02}/I_{01} (red/orange ratio). If the lifetimes and red/orange ratio are large, the quantum efficiency must be high. So, the different composition of the hybrid materials may have an influence on the luminescent lifetimes and quantum efficiencies.

β-diketones are already well-known to be good chelating ligands to sensitize luminescence of rare earth complexes [40–42]. The mechanism usually described for sensitized emission in rare-earth chelates proceeds through the following steps: (i) absorption via a ground singlet-excited singlet transition, (ii) radiationless intersystem crossing from the excited singlet to the triplet state, (iii) ligand-to-metal energy transfer to excited metal ion states, and (iv) lanthanide ions emission from the excited states [43–45]. According to Sato's result [46], the intramolecular energy migration efficiency from organic ligands to the central RE^{3+} is the most important factor determining the luminescence properties of lanthanide complexes. So, there should exist an optimal energy difference between the triplet-state position of organic ligands and the emissive energy level of RE^{3+} ions; a larger value for the equation and a smaller value for the energy difference will decrease the luminescence properties of rare-earth complexes. Thus, the energy difference between the lowest triple state energy of the ligand ($20\,400\,cm^{-1}$ for TTA, $24\,000\,cm^{-1}$ for DBM) and the resonance energy levels of Eu^{3+} ($^5D_1$, $19\,020\,cm^{-1}$), Tb^{3+} ($^5D_4$, $20\,500\,cm^{-1}$) were calculated, and it can be predicted that the triplet state energy of the ligand TTA is more suitable for the luminescence of Eu^{3+} ion than that of ligand DBM, While the ligand DBM has a better energy match to the luminescence of Tb^{3+} comparing with ligand TTA. The above emission spectra obtained from europium and terbium hybrids further demonstrate our predicted conclusion. Besides, the luminescent behavior is originated from the whole energy absorption and energy transfer, which as well depends on the intramolecular energy transfer from the charge transfer state (CTS) since the CTS appears in the excitation spectra of these hybrids. Faustino et al. [47] have given the theoretical approach analysis on the intramolecular energy transfer mechanism through CTS and Carlos et al. [48] have further applied this approach in the discussion of energy transfer mechanisms in europium (III) organic–inorganic hybrids systems. We selectively determined the energy transfer efficiency for the four covalently bonded mesoporous hybrid materials. The whole intramolecular energy transfer efficiencies within these hybrids are bpy-Eu-TTA-S16 (76%) and bpy-Eu-DBM-S16 (86%), respectively.

4. Conclusions

In summary, novel rare earth luminescent mesoporous hybrid materials bpy-*RE*-TTA-S16 and bpy-*RE*-DBM-S16 (*RE*=Eu, Tb) were successfully prepared by linking ternary rare earth (Eu^{3+}, Tb^{3+}) complexes to the order mesoporous SBA-16 through the functionalized β-diketone ligands (TTA-Si and DBM-Si), which provides a representative method for assembling mesoporous luminescent rare earth molecular-based hybrid materials with chemical bonds. All hybrid materials were characterized in detail, ranging from structures to properties. The results show that they all preserve their mesoscopically ordered structures and show highly uniform

pore size distributions. Further investigation on the luminescence properties show that the hybrid bpy-Eu-TTA-S16 present stronger luminescence intensity and longer lifetime than DBM-containing hybrid bpy-Eu-DBM-S16, while the hybrid bpy-Tb-DBM-S16 exhibit the stronger characteristic emission of Tb^{3+} and longer lifetime than the corresponding TTA-containing materials bpy-Tb-TTA-S16. In conclusion, all the data show that SBA-16, which presents a cage-like of uniform mesopore structure, is a good candidate host for supporting the lanthanide complex.

Acknowledgments

This work was supported by the National Natural Science Foundation of China (20971100) and Program for New Century Excellent Talents in University (NCET-08-0398).

Appendix A. Supplementary material

Supplementary data associated with this article can be found in the online version at doi:10.1016/j.jssc.2010.02.006.

References

[1] C. Molina, K. Dahmouche, C.V. Santilli, A.F. Craievich, S.J.L. Ribeiro, Chem. Mater. 13 (2001) 2818–2823.
[2] T. Suratwala, Z. Gardlund, K. Davidson, D.R. Uhlmann, Chem. Mater. 10 (1998) 190–198.
[3] H.R. Li, N.N. Lin, Y.G. Wang, Y. Feng, Q.Y. Gan, H.J. Zhang, Q.L. Dong, Y.H. Chen, Eur. J. Inorg. Chem. (2009) 519–523.
[4] B. Lebeau, C.E. Fowler, S.R. Hall, J. Mater. Chem. 9 (1999) 2279–2281.
[5] L.R. Matthews, E.T. Knobbe, Chem. Mater. 5 (1993) 1697–1700.
[6] J.L. Liu, B. Yan, J. Phys. Chem. C 112 (2008) 14168–14178.
[7] P. Lenaerts, A. Storms, J. Mullens, J. D'Haen, C. Görller-Walrand, K. Binnemans, K. Driesen, Chem. Mater. 17 (2005) 5194–5201.
[8] L.D. Carlos, R.A.S. Ferreira, V.D. Bermudez, S.J.L. Ribeiro, Adv. Mater. 21 (2009) 509–534.
[9] K. Binnemans, Chem. Rev. 109 (2009) 4283–4374.
[10] J.M. Lehn, Angew. Chem. Int. Ed. 29 (1990) 1304–1319.
[11] M.T. Murtagh, H.C. Kwon, M.R. Shahriari, M. Krihak, D.E. Ackley, J. Mater. Res. 13 (1998) 3326–3331.
[12] J. Gracia, M.A. Mondragon, C. Tellez, A. Campero, V.M. Castano, Mater. Chem. Phys. 41 (1995) 15–17.
[13] L.D. Carlos, R.A.S. Ferreira, J.P. Rainho, V.D. Bermudez, Adv. Funct. Mater. 12 (2002) 819–823.
[14] K. Binnemans, P. Lenaerts, K. Driesen, C. Görller-Walrand, J. Mater. Chem. 14 (2004) 191–195.
[15] Q.M. Wang, B. Yan, J. Photochem. Photobiol. A Chem. 178 (2006) 70–75.
[16] B. Yan, D.J. Ma, J. Solid State Chem. 179 (2006) 2059–2066.
[17] Q.M. Wang, B. Yan, J. Organomet. Chem. 691 (2006) 3567–3573.
[18] Q.M. Wang, B. Yan, J. Mater. Chem. 14 (2004) 2450–2454.
[19] Y.J. Li, B. Yan, Y. Li, Micropor. Mesopor. Mater. doi:10.1016/j.micromeso.2009.12.006.
[20] Y. Li, B. Yan, H. Yang, J. Phys. Chem. C. 112 (2008) 3959–3968.
[21] Y.J. Li, B. Yan, Inorg. Chem. 48 (2009) 8276–8285.
[22] J. Feng, S.Y. Song, Y. Xing, H.J. Zhang, Z.F. Li, L.N. Sun, X.M. Guo, W.Q. Fan, J. Solid State Chem. 182 (2009) 435–441.
[23] Y. Li, B. Yan, Dalton Trans. 39 (2010) 1480–1487.
[24] L.L. Kong, B. Yan, Y. Li, J. Solid State Chem. 182 (2009) 1631–1637.
[25] Y. Sakamoto, M. Kaneda, O. Terasaki, D.Y. Zhao, J.M. Kim, G.D. Stucky, H.J. Shin, R. Ryoo, Nature 408 (2000) 449–453.
[26] Y.J. Li, B. Yan, Dalton Trans. doi:10.1039/b919008b.
[27] G. Chandrasekar, K.S. You, J.W. Ahn, W.S. Ahn, Micropor. Mesopor. Mater. 111 (2008) 455–462.
[28] W.J. Son, J.S. Choi, W.S. Ahn, Micropor. Mesopor. Mater. 113 (2008) 31–40.
[29] Z. Wang, J. Wang, H.J. Zhang, Mater. Chem. Phys. 87 (2004) 44–48.
[30] H.F. Lu, B. Yan, J.L. Liu, Inorg. Chem. 48 (2009) 3966–3975.
[31] K. Binnemans, P. Lenaerts, K. Driesen, C. Gorller-Walrand, J. Mater. Chem. 14 (2004) 191–201.
[32] O.L. Malta, H.F. Brito, J.F.S. Menezes, F.R.G.E. Silva, S. Alves, F.S. Farias, A.V.M. Andrade, J. Lumin. 75 (1997) 255–268.
[33] C.Y. Peng, H.J. Zhang, J.B. Yu, Q.G. Meng, L.S. Fu, H.R. Li, L.N. Sun, X.M. Guo, J. Phys. Chem. B. 109 (2005) 15278–15287.
[34] P.C.R. Soares-Santos, H.I.S. Nogueira, V. Félix, M.G.B. Drew, R.A.S. Ferreira, L.D. Carlos, T. Trindade, Chem. Mater. 15 (2003) 100–108.
[35] R.A.S. Ferreira, L.D. Carlos, R.R. Goncalves, S.J.L. Ribeiro, V.D. Bermudez, Chem. Mater. 13 (2001) 2991–2998.
[36] E.E.S. Teotonio, J.G.P. Espínola, H.F. Brito, O.L. Malta, S.F. Oliveira, D.L.A.D. Foria, C.M.S. Izumi, Polyhedron 21 (2002) 1837–1844.
[37] L.D. Carlos, Y. Messaddeq, H.F. Brito, R.A. Sá Ferreira, V.D. Bermudez, S.J.L. Ribeiro, Adv. Mater. 12 (2000) 594–598.
[38] M.F. Hazenkamp, G. Blasse, Chem. Mater. 2 (1990) 105–110.
[39] M.H.V. Werts, R.T.F. Jukes, J.W. Verhoeven, Phys. Chem. Chem. Phys. 4 (2002) 1542–1548.
[40] F.S. Richardson, Chem. Rev. 82 (1982) 541–552.
[41] N. Sabbatini, M. Guardigli, J.M. Lehn, Coord. Chem. Rev. 123 (1993) 201–228.
[42] B. Yan, X.F. Qiao, J. Phys. Chem. B. 111 (2007) 12362–12374.
[43] G.A. Crosby, R.E. Whan, R.E. Alire, J. Chem. Phys. 34 (1961) 743–748.
[44] O.L. Malta, J. Lumin. 71 (1997) 229–236.
[45] O.L. Malta, Spectrochim. Acta Part A 54 (1998) 1593–1599.
[46] S. Sato, M. Wada, Bull. Chem. Soc. Jpn. 43 (1970) 1955–1966.
[47] W.M. Faustino, O.L. Malta, G.F. de Sa, J. Chem. Phys. 122 (2005) 054109-054109-10.
[48] P.P. Lima, S.S. Nobre, R.O. Freire, S.A. Junior, R.A.S. Ferreira, U. Pischel, O.L. Malta, L.D. Carlos, J. Phys. Chem. C 111 (2007) 17627–17634.